Orthogonal acoustic dimensions define auditory field maps in human cortex

Brian Barton[a], Jonathan H. Venezia[a,b], Kourosh Saberi[a,b], Gregory Hickok[a,b], and Alyssa A. Brewer[a,1]

[a]Center for Cognitive Neuroscience and Department of Cognitive Sciences, and [b]Center for Language Science and Center for Hearing Research, University of California, Irvine, CA 92697

Edited* by George Sperling, University of California, Irvine, CA, and approved November 1, 2012 (received for review August 16, 2012)

The functional organization of human auditory cortex has not yet been characterized beyond a rudimentary level of detail. Here, we use functional MRI to measure the microstructure of orthogonal tonotopic and periodotopic gradients forming complete auditory field maps (AFMs) in human core and belt auditory cortex. These AFMs show clear homologies to subfields of auditory cortex identified in nonhuman primates and in human cytoarchitectural studies. In addition, we present measurements of the macrostructural organization of these AFMs into "clover leaf" clusters, consistent with the macrostructural organization seen across human visual cortex. As auditory cortex is at the interface between peripheral hearing and central processes, improved understanding of the organization of this system could open the door to a better understanding of the transformation from auditory spectrotemporal signals to higher-order information such as speech categories.

tonotopy | periodotopy | cochleotopy | temporal receptive field | traveling wave

Humans have evolved a highly sophisticated auditory system for the transduction and analysis of acoustic information, such as the spectral content of sounds and the temporal modulation of sound energy. The basilar membrane of the cochlea is organized tonotopically to represent the spectral content of sounds from high to low frequencies. This tonotopic (or cochleotopic) organization is preserved as auditory information is processed and passed on from the cochlea to the superior olive, the inferior colliculus, the medial geniculate nucleus, and into primary auditory cortex. Such cortical preservation of the peripheral sensory topography creates a common topographic sensory matrix in hierarchically organized sensory systems, important for consistent sensory computations. The current state of knowledge of the functional organization of human auditory cortex indicates the existence of multiple cortical subfields organized tonotopically. However, the number of these human cortical subfields, their boundaries, and their orientations relative to anatomical landmarks remain equivocal, due in part to an inability to measure cortical representations of a second acoustic dimension orthogonal to tonotopy to accurately delineate them.

This ambiguity of human auditory subfield definitions contrasts dramatically with the current understanding of the functional organization of human visual cortex, in which detailed maps of the organization of the retina, called visual field maps (VFMs), have been well characterized (1–9). In vision, there are two orthogonal dimensions of visual space, eccentricity and polar angle, which together allow for the mapping of cortical representations to unique locations in visual space and the complete delineation of the boundaries of individual visual field maps. In audition, there has been only one dimension of sensory topography clearly mapped in cortex, which makes it impossible to use sensory topography to accurately differentiate specific human cortical auditory field maps (AFMs). Current estimates of human AFMs rely primarily on a monkey model that is well characterized by cytoarchitectonics (10, 11), single- and multiunit physiology (12–16), tracer studies (17), and functional magnetic resonance imaging (fMRI) (18). Human cytoarchitectonic measurements generally resemble those in macaque monkey and indicate that the small subfields of primary auditory cortex are confined to Heschl's gyrus (HG; or between HG-1 and HG-2, in cases where a double gyrus exists) and oriented medial to lateral along HG (19–22). However, these human cytoarchitectural measurements contrast greatly with the orientations and sizes of auditory field maps reported in fMRI studies. Indeed, human fMRI studies have had great difficulty localizing even primary auditory cortex, placing A1 anywhere from the medial aspect of HG (23), to its posterior sulcus (24–26), to planum temporale (27, 28).

Recently, representations of an acoustic dimension orthogonal to tonotopy, known as periodotopy, have been observed in cat primary auditory cortex (29) and the macaque midbrain (30). Following the established terminology, periodicity refers to the preferred temporal receptive field over which an auditory neuron operates, measured here by presenting broadband noise to the auditory system at different modulation rates. Thus, a periodotopic map is an orderly map organized from short temporal receptive fields (high-frequency periodicity) to long temporal receptive fields (low-frequency periodicity). A similar map exists for spatial receptive fields in vision, moving in an orderly fashion from small receptive fields in the fovea to large receptive fields in the periphery, parallel to the sensory space dimension of eccentricity (1–9).

The primary question addressed presently is whether the core and belt auditory cortex in human is organized with a microstructure of orthogonal tonotopic and periodotopic gradients that form complete AFMs. Recent human psychophysical studies have demonstrated that there are separable filter banks (receptive fields) for spectral and temporal information, as would be predicted by the existence of AFMs with orthogonal tonotopic and periodotopic gradients, respectively (31–33). However, to date, the only human study indicating the existence of orthogonal tonotopic and periodotopic representations in cortex uses magnetoencephalography (MEG) source localization at a scale that is impossible to localize to any one auditory subfield (34). Here, we report conclusive fMRI evidence for the existence of orthogonal tonotopic and periodotopic gradients forming complete AFMs in human core and belt auditory cortex. The presence of orthogonal gradients allowed the identification of 11 maps consistent with the human cytoarchitectural measurements (19–22) and with proposed homology to the 11 core and belt auditory subfields in macaque auditory cortex (10, 11, 17, 18). More broadly, we found that the 11 AFMs are organized into the radially orthogonal "clover leaf" clusters, similar to what has been reported as an organizing principle of VFMs in human visual cortex (4, 6, 7, 9, 35–37).

Results

FMRI Measurements of Tonotopy and Periodotopy. To measure human tonotopic and periodotopic gradients, we had four subjects undergo two fMRI scanning sessions on a 3T Philips Achieva scanner. For each subject, we collected one T1-weighted anatomical volume (3D MPRAGE, 1 mm^3 voxels, TR = 8.4 ms,

Author contributions: B.B., J.H.V., K.S., G.H., and A.A.B. designed research; B.B. and J.H.V. performed research; B.B. and A.A.B. analyzed data; and B.B. wrote the paper.

The authors declare no conflict of interest.

*This Direct Submission article had a prearranged editor.

[1]To whom correspondence should be addressed. E-mail: aabrewer@uci.edu.

This article contains supporting information online at www.pnas.org/lookup/suppl/doi:10.1073/pnas.1213381109/-/DCSupplemental.

Downloaded by guest on November 27, 2020

TE = 3.7 ms, flip = 8°, SENSE factor = 2.4), one T1-weighted in-plane anatomical scan to align the functional and anatomical data (1 × 1 × 3 mm voxels), and 12–16 functional auditory field mapping scans (T2-weighted, gradient echo imaging, TR = 10s, TA = 2s, TE = 30 ms, flip = 90°, SENSE factor = 1.7, reconstructed voxel size of 1.875 × 1.875 × 3 mm, no gap), with six to eight scans of narrowband noise for tonotopy in one session and six to eight scans of broadband noise for periodotopy in the other (*SI Text*).We used narrowband noise instead of pure tones because it has been demonstrated that narrowband noise in monkey fMRI drives voxels in auditory belt regions more robustly than do pure tones, without any cost in responses in auditory core (18, 38). Our broadband noise stimuli were similarly modeled after those used in previous studies [Fig. 1 and Fig. S1 (29, 30, 34)].

In both cases, we used a version of the standard procedure in visual field mapping, the traveling wave method (1–6, 7, 9), modified to a sparse sampling procedure to avoid data contamination due to scanner noise [Fig. 1 and Figs. S1 and S2 (39)]. In brief, each stimulus of a given type, narrowband or broadband, was presented in a block at a single value of center frequency or modulation rate, respectively. For tonotopic mapping, stimuli consisted of 100-Hz-wide bands of AM noise centered at 400; 800; 1,600; 3,200; and 6,400 Hz, and amplitude modulated at 8 Hz. Stimuli used for periodotopic mapping were broadband noise (0–8,000 Hz) modulated at 2, 4, 8, 16, 32, 64, 128, and 256 Hz (Fig. 1, Figs. S1 and S2, and *SI Text*). The entire range of stimuli was covered by consecutive blocks presented in order from low to high in what is referred to as one stimulus cycle. Six stimulus cycles were presented sequentially in each functional scan, and the blood-oxygen level-dependent (BOLD) percent modulation

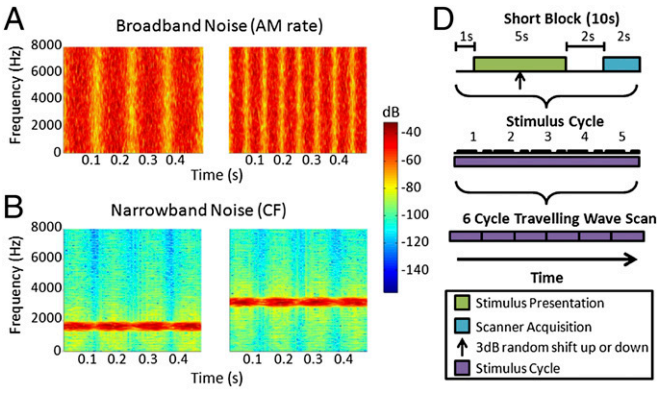

C

	Broadband Noise		Narrowband Noise	
Stimulus	Frequency Range (Hz)	Periodicity (AM rate, Hz)	Frequency Range (Hz)	Periodicity (AM rate, Hz)
1	0-8000	2	350-450	8
2	0-8000	4	750-850	8
3	0-8000	8	1550-1650	8
4	0-8000	16	3150-3250	8
5	0-8000	32	6350-6450	8
6	0-8000	64	N/A	N/A
7	0-8000	128	N/A	N/A
8	0-8000	256	N/A	N/A

Fig. 1. Experimental stimuli and design. The sound spectrogram across frequencies (vertical axes) and time (horizontal axes). Increasing sound energy is represented as increasingly "warmer" colors. (*A*) Example broadband noise stimuli with amplitude modulation (AM) rates of 8 (*Left*) and 16 Hz (*Right*). (*B*) Example narrowband noise stimuli with center frequencies (CF) of 1,600 (*Left*) and 3,200 Hz (*Right*). (*C*) All experimental stimuli. Broadband noise stimuli maintain constant frequency information and vary periodicity, whereas narrowband noise stimuli hold periodicity constant and vary frequency. (*D*) Sparse sampling traveling wave experimental design (*SI Text* and Fig. S1).

time series for all six to eight functional scans for each subject were averaged together. Finally, a Fourier coherence analysis was applied to every voxel to separate activity due to the stimuli (at the frequency of six cycles per scan) from activity due to random and physiological noise (at the other frequencies in the cycles per scan domain). The phase assigned to each voxel with activity above a standard coherence threshold of 0.20 corresponds to that voxel's preferred point in the relevant stimulus space (e.g., a given voxel's phase may indicate that it is preferentially tuned to the 1,600-Hz-centered narrowband noise stimulus over the other narrowband stimuli). AFMs were then defined individually for each hemisphere of each subject on a flattened representation of his/her cortex centered on HG (*SI Text*).

Tonotopic Organization. Our tonotopic measurements largely replicated the broad pattern of cortical organization reported in previous human studies (Fig. 2 *A*–*C* and Figs. S3*A* and *B* and S4*A* (19–28)]. A general and consistent pattern of tonotopic responses included a large low-frequency region oriented parallel to Heschl's gyrus, which was encircled by and transitioned to a high-frequency region. Without additional information, this broad pattern could be interpreted as a frequency reversal gradient running perpendicular to Heschl's gyrus, as some authors have proposed based on human fMRI measurements (23–28).

Periodotopic Organization. Periodotopic maps were clearly identified in all hemispheres of all subjects (Fig. 2 *A*, *B,* and *D* and Figs. S3 *C* and *D* and S4*B*). Visual inspection of these maps reveals that (*i*) orderly transitions through the modulation range are evident, (*ii*) the maps are clearly distinct from the tonotopic maps, and (*iii*) consistent organizational patterns exist across hemispheres and subjects. For example, a region of middle-high periodic modulation rates (32–64 Hz, cyan/green in Fig. 2*D* and Fig. S3 *C* and *D*) is evident in the posterior-medial portion of Heschl's gyrus, and "isoperiodotopic" bands tend to be organized in radial spokes within Heschl's gyrus.

Orthogonal Gradients Reveal 11 Cortical AFMs. By combining the tonotopic and periodotopic maps; i.e., using reversals in tonotopic maps to define one set of functional boundaries (solid lines in Fig. 2 *C* and *D* and Figs. S3 and S4) and using reversals in periodotopic maps to define another set of functional boundaries (dotted lines in Fig. 2 *C* and *D* and Figs. S3 and S4), we were able to identify 11 AFMs with orthogonal gradients in each subject. These 11 AFMs correspond nicely to proposed auditory fields in macaque auditory core and belt, suggesting that the 11 AFMs are the human homologs to the macaque fields. Our definitions of human AFMs follow the current macaque model of the organization of auditory core and belt, which is based upon cytoarchitectural, connectivity, and tonotopic measurements [See Fig. S7 (10, 11, 17, 18)]. Although no periodotopic gradients have been observed in primate cortex, it remains an empirical question—to our knowledge, no periodotopic stimuli have been used in a study of monkey core or belt. However, orthogonal periodotopic and tonotopic gradients have been observed in the macaque midbrain (30), strongly suggesting that this organization is preserved at least as far up the hierarchy as monkey core and belt and likely beyond, as we have measured here in human auditory cortex. We shall refer to our human AFMs as hA1, hR, hRT, hCM, hMM, hRM, hRTM, hCL, hAL, hRL, and hRTL, where "h" stands for "human" and the other letters simply indicate proposed homology but not the original physical relationships indicated by the monkey auditory subfield names (e.g., "hR" is simply "human R," not short for "human rostral"). Thus, hR is the proposed human homolog to R, or rostral, but because hR is actually lateral to hA1 in human, whereas R is rostral to A1 in monkey; our labels should not be taken to reflect the human anatomical orientation.

Every presently measured AFM has a very similar smooth, orderly progression of voxels spanning the tested range of tonotopy and periodotopy, with the dimensions represented (*i*) orthogonal to one another, as predicted by measurements in the

Downloaded by guest on November 27, 2020

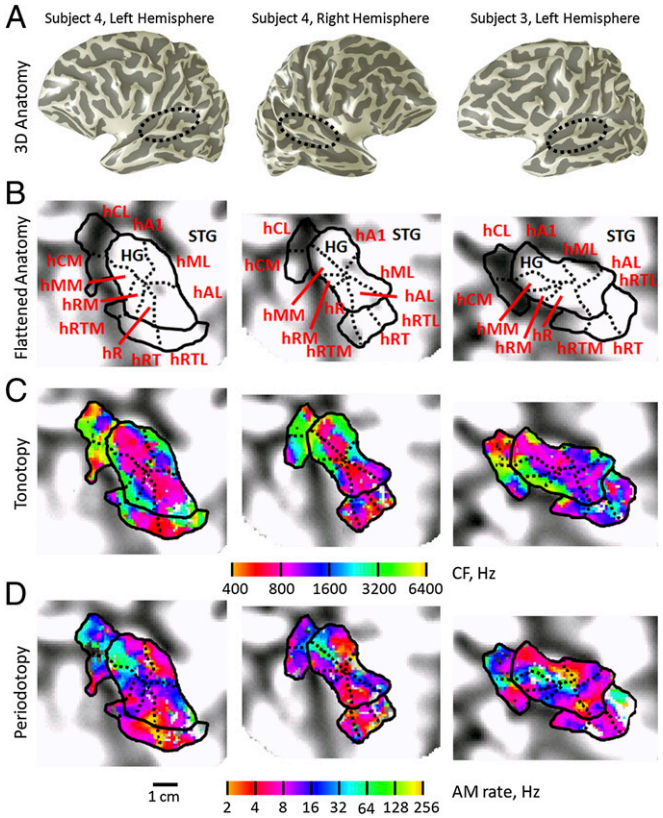

Fig. 2. Anatomical and functional data in auditory core and belt. (*Left*) Data in subject 4's (S4's) left hemisphere and (*Middle*) in S4's right hemisphere. (*Right*) Data in S3's left hemisphere. Light gray indicates gyri; dark gray indicates sulci. (*A*) A 3D rendering of individual cortical surfaces. Circles indicate HG and surrounding regions presented in (*B*). (*B*) Flattened cortical surface of HG and surrounding regions for each hemisphere, orientated to align STG. Solid black lines indicate AFM boundaries between maps along mirror-symmetric tonotopic reversals, which separate clover leaf clusters from one another. Dotted black lines indicate AFM boundaries between maps within a clover leaf cluster, in mirror-symmetric periodotopic reversals. Red text indicates AFM names; black text indicates gyri names. (*C*) Tonotopy mapped using narrowband noise stimuli. Colors indicate the preferred frequency range for each voxel (CF, in hertz). (*D*) Periodotopy mapped using broadband noise stimuli. Colors indicate the preferred period range for each voxel (AM rate, in hertz). Each voxel is measured independently with no spatial or temporal smoothing and no motion correction. Voxels presented have coherence above the statistical threshold of 0.20 and are within one of the 11 AFMs presently studied. Scale bar denotes 1 cm along the flattened cortical surface.

macaque midbrain [Figs. 2 and 3 (30)]. We considered the alternative possibilities that the tonotopic and periodotopic gradients could be distributed (*ii*) randomly, (*iii*) in parallel, or (*iv*) anti-parallel. To differentiate between these possibilities, for each map in each hemisphere of each subject, we located the center of the region representing the highest and lowest stimulus values for the tonotopic (400 and 6,400 Hz) and periodotopic (2 and 256 Hz) gradients. We then used these endpoints to create two vectors running from lowest to highest stimulus value, one for tones and one for periods, for each map. Maps with orthogonal gradients (*i*) should have vectors of this variety offset rotationally by about 90° from one another, whereas randomly distributed gradients (*ii*) should have no consistent arrangement (high SE, no meaningful average), parallel gradients should have no difference (0°) in vector offset (*iii*) and anti-parallel gradients should be 180° offset (*iv*). A multivariate analysis of variance (MANOVA) was performed with the null hypothesis for each AFM that the gradient vectors were orthogonal (offset by 90°; *i*) and the alternative hypothesis that they were randomly distributed (*ii*), parallel (0° offset; *iii*) or antiparallel (180° offset; *iv*). The result of the MANOVA failed to reject the null hypothesis that the gradient vectors as a whole were offset by 90° (orthogonal; *i*), $F(3,1) = 16.344$, $P = 0.179$. Post hoc, a univariate analysis of variance (ANOVA) was performed on each of the 11 AFMs, with the same null and alternative hypotheses as the MANOVA. Each ANOVA was corrected for multiple comparisons (Bonferroni, alpha = 0.0045), but we note that the results would be unchanged with 11 times the power at an uncorrected alpha = 0.05. The results of all 11 ANOVAs failed to reject the null hypothesis that the gradient vectors for each AFM were offset by 90° (orthogonal; *i*), with $F(3,1)$ values ranging from 2.113 to 14.450 and a corresponding range of P values from 0.860 to 0.112. Thus, we report that the gradient vectors for all 11 maps, averaged across hemispheres and subjects, are rotated about 90° from one another, consistent with orthogonal (*i*) tonotopic and periodotopic gradients (Fig. 3).

As an additional test for orthogonal tonotopic and periodotopic gradients independent of physical location, we compared the dispersion of tonotopic and periodotopic responses across all 11 measured maps (Fig. 4 and Fig. S5). If the tonotopic and periodotopic gradients are orthogonal (*i*), we should expect that in a subset of voxels of any given narrow range of tonotopy, the entire range of periodotopy should be represented (e.g., voxels within the subset that responds best to 400–800-Hz narrowband noise should also have responses spanning the entire range of broadband noise, 2–256 Hz). Conversely, in any given narrow range of periodotopy, the entire range of tonotopy should be represented (e.g., voxels within the subset that responds best to 8–16-Hz broadband noise should also span the entire range of narrowband noise, 400–6,400 Hz). If the tonotopic and periodotopic gradients are randomly distributed (*ii*), there should be no predictable pattern in the responses. If the gradients are parallel (*iii*) or antiparallel (*iv*), any given narrow range of tonotopy should correspond to a narrow range of periodotopy, and vice versa (e.g., the subset of voxels that responds best to 400–800-Hz narrowband noise may also respond best to only 2–4-Hz broadband noise, but not the entire periodotopic range, 2–256 Hz). As predicted, the pattern of responses in all hemispheres of all subjects is consistent with orthogonal (*i*) tonotopic and periodotopic gradients (Fig. 4 and Fig. S5).

Such an orthogonal organization of tonotopic and periodotopic gradients means that all voxels tuned to a particular tone span the range of temporal receptive fields represented within that particular AFM, and all voxels tuned to a particular temporal receptive field span the range of tones, such that all unique combinations of tonotopy and periodotopy are represented in any given AFM. As with VFMs in visual cortex, the similarity of this orthogonal pattern across AFMs is indicative of a common topographical sensory matrix across maps, over which different computations can be performed. This matrix naturally allows for feedforward and feedback communication between AFMs without complicated transformations as information travels up or down the processing hierarchy. Furthermore, this matrix framework allows for the parallel processing, and thus differentiation, of multiple auditory sources by their spectral contents in the temporal and tonotopic domains. Finally, as a practical matter for auditory researchers, orthogonal gradients allow for the unambiguous individuation of AFMs using fMRI. With just one gradient dimension, such as tonotopy, there are a number of nearby gradients that run together, and the localization of the boundaries specific to A1 or R, for example, becomes a matter of subjective interpretation. All previous studies of tonotopic responses on HG in humans have very similar data, but each interprets their data differently, leading to highly ambiguous and variable localization of individual auditory subfields (23–28). Those studies largely agree that human auditory core is on HG, but disagree on precisely where each subfield is, and even how many there are (23–28). The small sizes of auditory subfields suggested in macaque data and human cytoarchitectural measurements have also been a confounding

Downloaded by guest on November 27, 2020

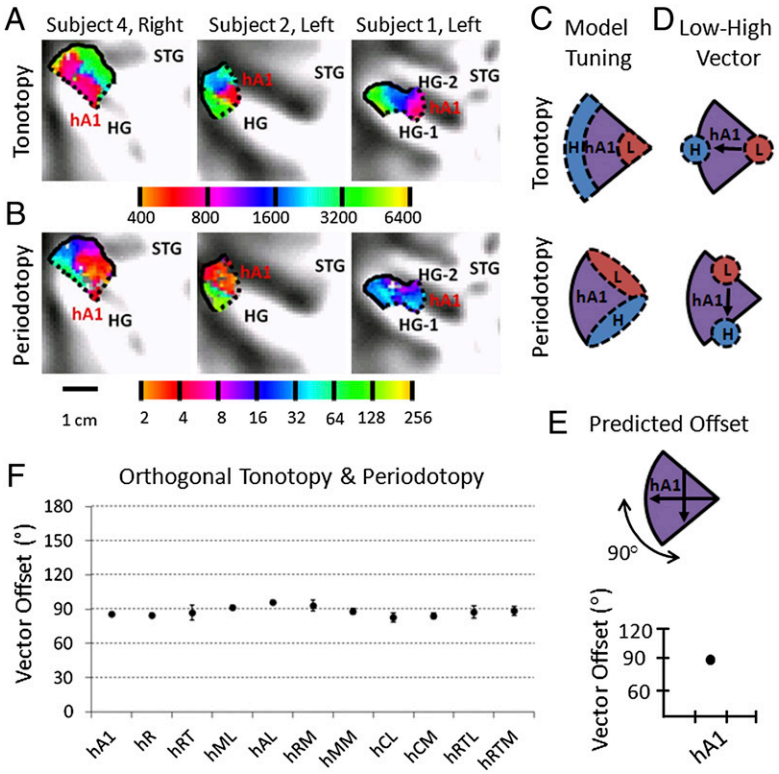

Fig. 3. Orthogonal tonotopic and periodotopic representations. (*A*) Tonotopy and (*B*) periodotopy. (*Left*) Data in S4's right hemisphere. (*Center*) Data in S2's left hemisphere. (*Right*) Data in S1's left hemisphere. (*Inset*) Scale bar denotes 1 cm along the flattened cortical surface for images in (*A*) and (*B*). Details of (*A*) and (*B*) as in Fig. 2. (*C*) Model tuning for tonotopy (*Top*) and periodotopy (*Bottom*) in hA1. Red regions indicate low stimulus values (e.g., low frequency for tonotopy or low-modulation rate for periodotopy); blue regions indicate high-stimulus values. (*D*) Vectors were drawn from centers of low-stimulus value region of interests (ROIs) to high stimulus value ROIs for tonotopy (*Top*) and periodotopy (*Bottom*). (*E*) Vector offset predicted by orthogonal tonotopic and periodotopic gradients physically (*Top*) and graphically (*Bottom*). (*F*) Results of the vector offset test for orthogonality for each AFM, averaged across all eight hemispheres. All maps have an offset of about 90°, confirming that the two gradients are orthogonal. Error bars indicate SEM.

factor in many of the human neuroimaging studies, which have had difficulty in measuring such small tonotopic gradients in individual subjects (23–28). Our present data reveal that there are 11 AFMs on or bordering HG that closely resemble the macaque model of auditory core and belt, and that it is necessary to measure both tonotopy and periodotopy to localize them accurately (Figs. 2 and 3). We provide the average surface areas and Talairach locations for each of the 11 AFMs in Fig. S6 and Table S1, respectively.

Restricting our microstructural analysis to the AFMs of the human auditory core, we find that they are effectively identical to those of macaque; all of the tonotopic boundary reversals between hCM/hCL and hA1; hA1 and hR; and hR and hRT predicted by the monkey core model can be identified in human core (Fig. 2 and Fig. S7). The anterior/medial aspect of hA1 is tuned to high tones and the posterior/lateral aspect is tuned to low tones (Figs. 2, 3, and 5 and Fig. S7). The high-tone region of hA1 abuts the high-tone regions of hCM and hCL, forming what is known as a boundary reversal between maps. Such reversals indicate the boundaries between hCM and hA1 (high tones), hCL and hA1 (high tones), hA1 and hR (low tones), and hR and hRT (high tones; Figs. 2 and 5 and Fig. S7). To date no such functional boundary has been identified between monkey core and belt maps, primarily because periodotopic gradients have so far only been measured in macaque midbrain (30). Instead, the macaque boundaries have been measured using cytoarchitectural differences, electrophysiological responses, and connectivity patterns (10, 11, 14–17) and roughly estimated when such information is not available (18).

The monkey model of the belt region, however, is inadequate to describe our tonotopic data in the human belt. Although we observe the expected tonotopic reversals between hCM and hMM; hCL and hML; hRM and hRTM; and hAl and hRTL, we do not detect a tonotopic reversal between hMM and hRM or hML and hAL. Instead, we measure periodotopic reversals between hMM and hRM and between hML and hAL. In addition, we observe periodotopic reversals between the human homolog to core and belt, or between hA1 and hMM; hA1 and hML; hR and hRM; hR and hAL; hRT and hRTM; and hRT and hRTL (Figs. 2 and 5 and Fig. S7).

Macrostructural Organization of Human AFMs. These patterns of the tonotopic and periodotopic gradients are well described by a clover leaf cluster organization such as the organizational pattern also measured by our laboratory and others for VFMs (4, 6, 7, 35–37, 40). A growing body of evidence on the macrostructure of VFMs in human (4, 6, 7, 9, 35–37) and macaque visual cortex (40) indicates that VFMs are organized into roughly circular clover leaf VFM clusters. VFMs in a clover leaf cluster are organized such that the central foveal representation of each VFM is positioned in the center of the cluster, with more peripheral representations of space represented in more peripheral positions in the cluster in a smooth, orderly fashion. The representation of any given polar angle of space for each VFM extends out from the center to the periphery of the clover leaf cluster, effectively spanning the radius of the cluster like a spoke on a wheel. This type of macrostructural organization—one dimension of sensory topography represented in radial bands from center to periphery of a cluster (periodicity for AFMs) and the other dimension represented in concentric, circular bands from center to periphery (tonotopy for AFMs)—is referred to as being radially orthogonal. Here, our measurements reveal that AFMs, like VFMs, have a roughly circular clover leaf cluster macrostructure that is very similar to the widely accepted monkey model of auditory core (10–12, 14–18) and both monkey and human VFM macrostructure [Figs. 2 and 5 and Fig. S7 (4, 6, 7, 35–37, 40)].

In the present AFM data, we observe one complete clover leaf cluster, which is centered on HG, containing the six AFMs hA1, hR, hMM, hRM, hML, and hAL (see *SI Text*). We refer to this clover leaf cluster as the HG cluster. The medial aspect of the HG cluster lies on the medial aspect of HG, abutting hCM and hCL, which extend onto the circular gyrus and medial wall of the Sylvian fissure, respectively. The lateral aspect of the HG cluster lies where HG meets the superior temporal gyrus (STG), abutting hRT, hRTM, and hRTL, which lie on the STG at the base of

Downloaded by guest on November 27, 2020

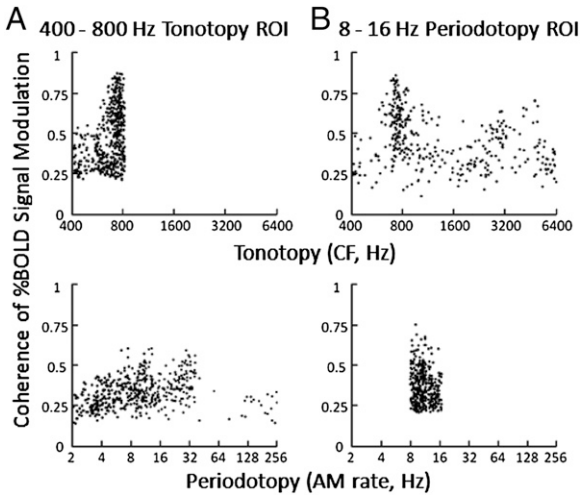

Fig. 4. Orthogonal tonotopy and periodotopy in narrow-range ROIs. Data are from ROIs defined across all 11 AFMs in S4's left hemisphere. Specific narrow-range ROIs were created from voxels with statistically significant activity (coherence ≥ 0.20) for a specific range (e.g., 400–800 Hz) of a stimulus type (e.g., tonotopy), as noted above each column. (*A*) The 400–800-Hz tonotopy ROI. (*B*) The 8–16-Hz periodotopy ROI. Plots show data for responses either for the defining stimulus type [narrow-range tonotopic responses (*Upper Left*); narrow-range periodotopic responses (*Lower Right*)] or for the orthogonal stimulus type [periodotopic responses within tonotopic-defined ROI (*Lower Left*); tonotopic responses within periodotopic-defined ROI (*Upper Right*)]. It is key to note that within each narrow-range ROI, the entire range of the other acoustic dimension is represented. These results further confirm that the tonotopic and periodotopic representations are orthogonal. See Fig. S5 for additional examples.

HG. The anterior and posterior aspects of the HG cluster are restricted to the sulci bordering HG, without extending into planum temporale (PT) or planum polare (PP; Figs. 2 and 5 and Fig. S7). In the center of the HG cluster lies the low-frequency tonotopic representation, with bands of progressively higher-frequency tonotopic tuning as one moves eccentric from the center of the cluster, until reaching the high-frequency tonotopic voxels at the outermost ring of the HG cluster. Each AFM within the HG cluster has a tonotopic gradient running from the center to the periphery of the cluster. Extending from the center of the HG cluster to its periphery are the isofrequency lines of periodotopic tuning, like the spokes on a wheel (Figs. 2 and 5 and Fig. S7). Each AFM within the HG cluster has a periodotopic gradient running from one spoke on the wheel, rotating around the cluster to another spoke on the wheel. We observe six periodotopic tuning reversals at the highest and lowest periodotopic frequencies, indicating the boundaries between the AFMs within the HG cluster. This is the radially orthogonal clover leaf cluster organization, with one dimension of our AFM (tonotopy) divided into roughly circular isotone bands around a center point and isoperiod bands of the orthogonal dimension (periodotopy) spanning from the center to periphery of the cluster. This arrangement requires that the individual AFMs be shaped like slices of pie.

To verify the proposed clover leaf cluster organization of the HG cluster, we tested whether the vectors previously used to test the orthogonality within individual AFMs were radially orthogonal. If the six maps are organized into a clover leaf cluster (*i*), we should expect that the "low" endpoint of each of the six tonotopic vectors (see above) should be located in the center of the HG cluster, with each vector pointing to the periphery of the HG cluster (running along a wheel spoke of the cluster). Furthermore, we should expect that the periodotopic vectors should be orthogonal to the tonotopic vectors (90° offset), running around the circular cluster (pointing roughly from the midpoint of one wheel spoke to the next). In contrast, if the maps are randomly oriented (*ii*), we should expect to see no discernible pattern in the tonotopic or periodotopic vectors. Alternatively, if the maps have parallel tonotopic gradients (*iii*), we should expect that the tonotopy vectors would be aligned (0° offset between maps) and the maps adjacent, forming a strip. Finally, if the maps have tonotopic gradients that are anti-parallel to one another (*iv*), we should expect that the tonotopy vectors would be 180° offset between maps and the maps adjacent in two strips, mirror-reversed. Situations (*iii*) and (*iv*) would force the orthogonal periodotopic vectors for each map to be anti-parallel to one another (180° offset between maps). Across all subjects and hemispheres, responses of the maps hA1, hMM, hRM, hR, hRL, and hML are consistent with the model of orthogonal (*i*) tonotopic and periodotopic gradients forming one clover leaf cluster, which we name the HG cluster (Figs. 2–5 and Figs. S3, S5, and S7). The maps hCM and hCL may form one half of another clover leaf cluster, as may the maps hRTM, hRT, and hRTL; however, that is beyond the scope of the present work.

Discussion

We have demonstrated that the human auditory core and belt are organized with a microstructure of orthogonal tonotopic and periodotopic gradients that form complete AFMs. Furthermore, we demonstrate that six of these AFMs form a clover leaf cluster called the HG cluster, centered on HG. It is likely that the AFMs surrounding the HG cluster are also roughly half of two additional clover leaf clusters, based on the prevalence of this type of organization in VFMs (4, 6, 7, 35–37, 40). Our results are consistent with predictions from the widely accepted macaque model of auditory core and belt, based on measurements of tonotopy, periodicity, cytoarchitecture, and connectivity (10–18). The present results are also consistent with the published data, although not necessarily the interpretation, of previous studies of tonotopic gradients in humans (23–28). Our results are consistent with work

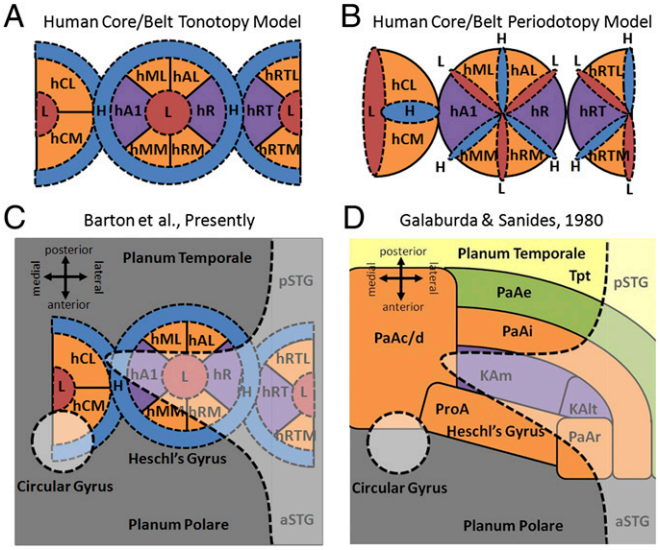

Fig. 5. Model of clover leaf cluster organization and comparison with human anatomy and cytoarchitecture. "L" stands for "low" and "H" stands for "high," referring to low (red regions) or high (blue regions) model tonotopic or periodotopic responses. Dark gray indicates sulci or the plane of the Sylvian fissure, while light gray indicates gyri. Purple regions represent auditory core. Orange regions indicate auditory belt. Green regions indicate auditory parabelt. Yellow regions indicate temporal planum temporal (Tpt). All figures are oriented along the same global axes (*Insets*). All models are representations of the original models cited above each figure, modified for consistency here. (*A*) Our human core/belt tonotopy model. (*B*) Our human core/belt periodotopy model. (*C*) Our tonotopic model of human belt and core. (*D*) Cytoarchitectonic model of human auditory cortex.

Downloaded by guest on November 27, 2020

on the cytoarchitecture of human auditory core and belt, unlike the myriad interpretations of the human tonotopic gradient neuroimaging data (19–22). Taken together with recent findings of clover leaf cluster organization of VFMs, our results suggest that this macrostructural organization is common to sensory systems, providing a basic framework for the complex processing and analysis of input from sensory receptors. In addition, the clover leaf cluster organization is key for minimizing the length of axons connecting between sensory maps within and between clusters, allowing for a more efficient ratio of brain matter–to-skull capacity.

Armed with this foundational knowledge of the number, location, and organization of AFMs in human auditory core and belt, future research can be directed to localizing higher-order AFMs and discerning which computations are performed in each AFM. For example, research on the neural basis of speech perception overwhelmingly emphasizes the identification of relatively higher-level auditory systems that are specialized for coding speech sound categories (phonemes). This work often compares the brain's response to speech versus various acoustic controls to factor out low-level acoustic processes. Although this is a valuable approach, it ignores the fact that the input to these higher-level systems derives from an acoustic signal that is already highly processed in the spectral and temporal domains. Understanding the nature of the inputs to higher-level speech perception systems is critical to understanding what kind of categorical information is ultimately extracted from the speech stream (which is still an open question) and how it is extracted computationally. The present work provides the foundation for such cortical measurements in the auditory systems of humans and nonhuman primates.

Methods

Subjects. Four people (one female and three males, aged 26–38) from the University of California, Irvine, served as participants for the present study. The experimental protocol was approved by the Institutional Review Board at University of California, Irvine, and informed consent was obtained from all subjects.

Experimental Design. Each subject underwent two functional magnetic resonance imaging (fMRI) scan sessions, which involved collecting a T1-weighted anatomical volume, a T1-weighted in-plane anatomical scan, and 12–16 functional auditory field mapping scans (For more information see *Results*, Fig. 1, *SI Text*, Figs. S1 and S2).

Auditory Field Mapping. The traveling wave method from standard fMRI paradigms for visual field mapping (1–3, 5, 7, 9, 41–45) was adapted for our sparse sampling auditory paradigm (For more information see *Results*, *SI Text*, Figs. S1–S4).

ACKNOWLEDGMENTS. This work was funded by National Institutes of Health Grant DC03681 (to G.H. and K.S.), a grant from the Center for Hearing Research at the University of California at Irvine (to G.H., A.A.B., and K.S.), and by University of California at Irvine, startup funds (to A.A.B.).

1. Engel SA, et al. (1994) fMRI of human visual cortex. *Nature* 369(6481):525.
2. Sereno MI, et al. (1995) Borders of multiple visual areas in humans revealed by functional magnetic resonance imaging. *Science* 268(5212):889–893.
3. DeYoe EA, et al. (1996) Mapping striate and extrastriate visual areas in human cerebral cortex. *Proc Natl Acad Sci USA* 93(6):2382–2386.
4. Brewer AA, Liu J, Wade AR, Wandell BA (2005) Visual field maps and stimulus selectivity in human ventral occipital cortex. *Nat Neurosci* 8(8):1102–1109.
5. Wandell BA, Winawer J (2011) Imaging retinotopic maps in the human brain. *Vision Res* 51(7):718–737.
6. Wandell BA, Brewer AA, Dougherty RF (2005) Visual field map clusters in human cortex. *Philos Trans R Soc London B Biol Sci* 360(1456):693–707.
7. Wandell BA, Dumoulin SO, Brewer AA (2007) Visual field maps in human cortex. *Neuron* 56(2):366–383.
8. Dumoulin SO, Wandell BA (2008) Population receptive field estimates in human visual cortex. *Neuroimage* 39(2):647–660.
9. Brewer AA, Barton B (2012) Visual field map organization in human visual cortex. *Visual Cortex - Current Status and Perspectives*, eds Molotchnikoff S, Rouat J (InTech, Croatia), pp 29–60.
10. Kaas JH, Hackett TA (1998) Subdivisions of auditory cortex and levels of processing in primates. *Audiol Neurootol* 3(2-3):73–85.
11. Kaas JH, Hackett TA (2000) Subdivisions of auditory cortex and processing streams in primates. *Proc Natl Acad Sci USA* 97(22):11793–11799.
12. Morel A, Garraghty PE, Kaas JH (1993) Tonotopic organization, architectonic fields, and connections of auditory cortex in macaque monkeys. *J Comp Neurol* 335(3): 437–459.
13. Merzenich MM, Brugge JF (1973) Representation of the cochlear partition of the superior temporal plane of the macaque monkey. *Brain Res* 50(2):275–296.
14. Kusmierek P, Rauschecker JP (2009) Functional specialization of medial auditory belt cortex in the alert rhesus monkey. *J Neurophysiol* 102(3):1606–1622.
15. Rauschecker JP, Tian B (2004) Processing of band-passed noise in the lateral auditory belt cortex of the rhesus monkey. *J Neurophysiol* 91(6):2578–2589.
16. Tian B, Rauschecker JP (2004) Processing of frequency-modulated sounds in the lateral auditory belt cortex of the rhesus monkey. *J Neurophysiol* 92(5):2993–3013.
17. de la Mothe LA, Blumell S, Kajikawa Y, Hackett TA (2006) Cortical connections of the auditory cortex in marmoset monkeys: Core and medial belt regions. *J Comp Neurol* 496(1):27–71.
18. Petkov CI, Kayser C, Augath M, Logothetis NK (2006) Functional imaging reveals numerous fields in the monkey auditory cortex. *PLoS Biol* 4(7):e215.
19. Fullerton BC, Pandya DN (2007) Architectonic analysis of the auditory-related areas of the superior temporal region in human brain. *J Comp Neurol* 504(5):470–498.
20. Galaburda A, Sanides F (1980) Cytoarchitectonic organization of the human auditory cortex. *J Comp Neurol* 190(3):597–610.
21. Rivier F, Clarke S (1997) Cytochrome oxidase, acetylcholinesterase, and NADPH-diaphorase staining in human supratemporal and insular cortex: Evidence for multiple auditory areas. *Neuroimage* 6(4):288–304.
22. Sweet RA, Dorph-Petersen KA, Lewis DA (2005) Mapping auditory core, lateral belt, and parabelt cortices in the human superior temporal gyrus. *J Comp Neurol* 491(3): 270–289.
23. Talavage TM, et al. (2004) Tonotopic organization in human auditory cortex revealed by progressions of frequency sensitivity. *J Neurophysiol* 91(3):1282–1296.
24. Humphries C, Liebenthal E, Binder JR (2010) Tonotopic organization of human auditory cortex. *Neuroimage* 50(3):1202–1211.
25. Woods DL, et al. (2010) Functional properties of human auditory cortical fields. *Front Syst Neurosci* 4:155.
26. Da Costa S, et al. (2011) Human primary auditory cortex follows the shape of Heschl's gyrus. *J Neurosci* 31(40):14067–14075.
27. Formisano E, et al. (2003) Mirror-symmetric tonotopic maps in human primary auditory cortex. *Neuron* 40(4):859–869.
28. Upadhyay J, et al. (2007) Function and connectivity in human primary auditory cortex: A combined fMRI and DTI study at 3 Tesla. *Cerebr Cortex* 17(10):2420–2432.
29. Langner G, Dinse HR, Godde B (2009) A map of periodicity orthogonal to frequency representation in the cat auditory cortex. *Front Integr Neurosci* 3:27.
30. Baumann S, et al. (2011) Orthogonal representation of sound dimensions in the primate midbrain. *Nat Neurosci* 14(4):423–425.
31. Dau T, Kollmeier B, Kohlrausch A (1997) Modeling auditory processing of amplitude modulation. II. Spectral and temporal integration. *J Acoust Soc Am* 102(5 Pt 1): 2906–2919.
32. Ewert SD, Dau T (2000) Characterizing frequency selectivity for envelope fluctuations. *J Acoust Soc Am* 108(3 Pt 1):1181–1196.
33. Hsieh IH, Saberi K (2010) Detection of sinusoidal amplitude modulation in logarithmic frequency sweeps across wide regions of the spectrum. *Hear Res* 262(1-2):9–18.
34. Langner G, Sams M, Heil P, Schulze H (1997) Frequency and periodicity are represented in orthogonal maps in the human auditory cortex: Evidence from magnetoencephalography. *J Comp Physiol A Neuroethol Sens Neural Behav Physiol* 181(6): 665–676.
35. Kolster H, Peeters R, Orban GA (2010) The retinotopic organization of the human middle temporal area MT/V5 and its cortical neighbors. *J Neurosci* 30(29):9801–9820.
36. Barton B, Brewer AA (2010) Pinwheel cartography: A fundamental organizing principle of the human visual system. *Neuroscience 2010 Abstracts* (Washington, DC: Society for Neuroscience), 19.11.
37. Brewer AA, Barton B (2011) 'Clover Leaf' cartography: Connectivity among visual field map clusters. *Neuroscience 2011 Abstracts* (Washington, DC: Society for Neuroscience) 851.801.
38. Miller GA, Taylor WG (1948) The perception of repeated bursts of noise. *J Acoust Soc Am* 20:171–182.
39. Petkov CI, Kayser C, Augath M, Logothetis NK (2009) Optimizing the imaging of the monkey auditory cortex: Sparse vs. continuous fMRI. *Magn Reson Imaging* 27(8): 1065–1073.
40. Kolster H, et al. (2009) Visual field map clusters in macaque extrastriate visual cortex. *J Neurosci* 29(21):7031–7039.
41. Maes F, Collignon A, Vandermeulen D, Marchal G, Suetens P (1997) Multimodality image registration by maximization of mutual information. *IEEE Trans Med Imaging* 16(2):187–198.
42. Teo PC, Sapiro G, Wandell BA (1997) Creating connected representations of cortical gray matter for functional MRI visualization. *IEEE Trans Med Imaging* 16(6):852–863.
43. Wandell BA, Chial S, Backus BT (2000) Visualization and measurement of the cortical surface. *J Cogn Neurosci* 12(5):739–752.
44. Dougherty RF, et al. (2003) Visual field representations and locations of visual areas V1/2/3 in human visual cortex. *J Vis* 3(10):586–598.
45. Nestares O, Heeger DJ (2000) Robust multiresolution alignment of MRI brain volumes. *Magn Reson Med* 43(5):705–715.

Downloaded by guest on November 27, 2020